Published in final edited form as:
J Endourol. 2003 September ; 17(7): 435–446.

Cavitation Bubble Cluster Activity in the Breakage of Kidney Stones by Lithotripter Shock Waves

Yuriy A. Pishchalnikov[1], **Oleg A. Sapozhnikov**[1], **Michael R. Bailey**[2], **James C. Williams Jr.**[3], **Robin O. Cleveland**[4], **Tim Colonius**[5], **Lawrence A. Crum**[2], **Andrew P. Evan**[3], and **James A. McAteer**[3]

1 *Department of Acoustics, Physics Faculty, M.V. Lomonosov Moscow State University, Moscow 119992, Russia (Tele: 7-095-939-2952; FAX: 7-095-932-8876)*

2 *Center for Industrial and Medical Ultrasound, Applied Physics Laboratory, University of Washington, Seattle, WA 98105, USA (Tele: 206-685-8618; FAX: 206-543-6785)*

3 *Department of Anatomy and Cell Biology, Indiana University School of Medicine, Indianapolis, IN 46202, USA (Tele: 317-274-7935; FAX: 317-278-2040)*

4 *Department of Aerospace and Mechanical Engineering, Boston University, Boston, MA 02215, USA (Tele: 617-353-7767; FAX: 617-353-5866)*

5 *Division of Engineering and Applied Science, California Institute of Technology, Pasadena, CA 91125, USA (Tele: 626-395-4021; FAX: 626-568-2719)*

Abstract

High-speed photography was used to analyze cavitation bubble activity at the surface of artificial and natural kidney stones during exposure to lithotripter shock waves *in vitro*. Numerous individual bubbles formed at the surface of stones, but these bubbles did not remain independent and combined with one another to form bubble clusters. Bubble clusters formed at the proximal end, the distal end, and at the sides of stones. Each cluster collapsed to a narrow point of impact. Collapse of the proximal cluster caused erosion at the leading face of the stone and the collapse of clusters at the sides of stones appeared to contribute to the growth of cracks. Collapse of the distal cluster caused minimal damage. We conclude that cavitation-mediated damage to stones was due not to the action of solitary bubbles, but to the growth and collapse of bubble clusters.

Keywords

shock wave lithotripsy; shock waves; cavitation; cavitation bubble clusters; kidney stones; high-speed photography

INTRODUCTION

Cavitation plays an important role in shock wave lithotripsy (SWL). There is strong evidence to show that cavitation bubble activity contributes to stone breakage[1–7] and recent studies support the idea that SW-bubble interactions are involved in the tissue trauma that occurs as a consequence of shock wave treatment.[8–13] The fact that cavitation appears to be linked both

Please send correspondence to: James A. McAteer, Ph.D., Department of Anatomy and Cell Biology, Indiana University School of Medicine, 635 Barnhill Drive (MS 5055), Indianapolis, IN 46202-5120, Telephone: 317-274-7935, FAX: 317-278-2040, mcateer@anatomy.iupui.edu.

to stone breakage and to adverse effects has fueled interest in research to determine the precise mechanisms of bubble action, and to efforts to find ways to control cavitation.

Several experimental findings help demonstrate the importance of cavitation in stone comminution. For example, placing a stone in a viscous medium[7,14,15] or covering the proximal face of the stone with a material that separates it from the surrounding fluid[14,16,17] reduces damage. Also, when stones are exposed to shock waves at overpressure sufficient to eliminate cavitation, they show no surface damage such as erosion or pitting, and the dose of shock waves needed to fracture the stones is substantially increased.[2,17] In addition, when stones are treated with shock waves in which the timing of the compressive and tensile components of the pressure pulse is reversed (thereby suppressing cavitation) damage is dramatically reduced.[11,18,19]

Cavitation control may be a way to improve lithotripsy. Studies with dual shock wave sources have shown that timing of the lithotripter pulses can be used to suppress or intensify cavitation. If the second pulse arrives while cavitation bubbles initiated by the first pulse are growing (~<100 μs) the bubble cycle is interrupted and bubble collapse is weak. If, however, the second pulse arrives as bubbles are inertially collapsing (~250–300 μs) bubble collapse is intensified and bubble-mediated damage is increased. An obvious goal is to find conditions that enhance cavitation at the stone, and thus enhance stone breakage, but suppress cavitation within tissue —making SW treatment safer and more effective. There has been good progress in this direction[6,20–22] and work is ongoing to discover the potential of such strategies. One part of this effort is continued research to better characterize the mechanisms of SW-stone interactions, to improve understanding of how cavitation bubbles cause damage.

Assessment of the role of cavitation in stone fragmentation is made difficult by the speed of the events involved. Shock wave propagation and cavitation bubble dynamics are fast processes measured from nanoseconds (e.g. rise time of the shock front) to several hundred microseconds (e.g. inertial bubble collapse). This means that some events occur faster than conventional methods of detection can resolve. Still, very useful information about cavitation dynamics has been obtained even from methods that are limited to quantitation of the damage produced by bubble collapse. For example, the spatial extent and intensity of cavitation can be measured using aluminum foil targets.[23–25] Some temporal features of cavitation can be monitored by fiber optic transmittance[26,27] and the intensity of cavitation bubble collapse has been characterized by monitoring sonoluminescence.[28–30] Laser scattering methods[31,32] have been used to measure time histories of bubble dynamics and passive cavitation detection using single or dual focused hydrophones has been used to detect inertial cavitation both *in vitro* and *in vivo*.[5,9,12,28,33]

High-speed photography has been very useful for understanding how cavitation bubbles interact with stones. The first high speed photographic observations of cavitation bubbles in the focus of a lithotripter provided dramatic visual evidence of the vast numbers of bubbles generated by each pressure pulse, and confirmed the fact that bubbles, indeed, interacted with the stone.[34] Since this initial report, various modes of high-speed photography have been utilized to study bubble activity. One method to capture rapid events is to use pulsed-laser stroboscopic illumination with a conventional camera.[13,35,36] The drawback of such a set-up is that only one frame per lithotripter pulse can be recorded. Stroboscopic movies can be made by changing the laser pulse delay relative to the lithotripter spark discharge and recording numerous shock waves. This approach has been used effectively to document bubble behavior in the free field,[37] to record the response of pre-existing bubbles in a silicone tubing blood vessel phantom,[13] and to capture simultaneously the shock wave stress fronts propagating within epoxy targets and profiles of the cavitation bubbles at the surface of these model stones.[36]

However, cavitation is not precisely repeatable from shock wave to shock wave.[28,33] Photographic reconstructions using the stroboscopic approach give a good estimate of cavitation but do not allow as complete an appreciation of the dynamics of bubble activity as is possible by capturing multiple frames over the course of a single lithotripter pulse. That is, there is information to be gained from recording changes in bubble form and position from moment to moment.

One advantage to be gained from this approach is a better understanding of bubble interactions in lithotripsy. Almost all cavitation modeling in lithotripsy considers the behavior of single, spherical bubbles that remain symmetrical.[38–43] Some photographic studies have also focused primarily on the behavior of single bubbles in order to allow comparison with these models.[13,36,44,45] But cavitation in lithotripsy involves more than single bubbles, and this is evident regardless of the mode of image capture.[15,32,34,36,42] Bubble-bubble interactions in the form of “bubble clouds” and “bubble clusters” have been shown to have a profound effect on cavitation dynamics in other systems.[46–50] It seems likely that bubble cluster dynamics will prove to be important in lithotripsy as well.[51] Indeed, recent computations of bubble clouds generated by lithotripter pulses[52] have shown similarly dramatic effects, including strong dependence of shock focusing and collapse dynamics on bubble number density.

In the present study we report our observations using a high-speed, multi-frame camera to record cavitation at the surface of artificial and natural kidney stones *in vitro*. Sequential frames were captured to document the bubble activity generated by single shock waves. The images show that cavitation at the surface of stones is in the form of bubble clusters and that violent cluster collapse contributes to stone breakage. These descriptive data should be useful as input for numerical modeling of bubble cluster collapse in SWL.

MATERIALS AND METHODS

High-speed camera

Images of cavitation bubbles at the surface of artificial and natural kidney stones were recorded using an Imacon-468 high speed digital camera (HS-camera)(DRS Hadland, Inc., Cupertino, CA). With this imaging system, seven 576×385 pixel frames could be recorded at speeds of up to 100 million frames per second. Inter-frame timing was adjustable (minimum 10 ns). Lighting was provided by a single high intensity xenon flash lamp of 1.5 millisecond duration with 1000 joules stored energy. Triggering was achieved using a photodiode to detect the light from the lithotripter spark discharge. Digital images were post-processed using Adobe Photoshop. Each image was adjusted using Auto Levels and sharpened using the Unsharp Mask filter (amount = 100%; radius = 4 pixels). More than 300 high-speed sequences (7 frames each) of bubble behavior at the surface of stones were recorded and analyzed by this method.

Lithotripter

Studies were conducted using a research electrohydraulic shock wave lithotripter that produces the same acoustic output as an unmodified Dornier HM3 clinical lithotripter (80 nF capacitor).[53] Electrohydraulic lithotripters employ an underwater spark discharge to produce a shock pulse. The spark discharge takes place at the internal focus (F1) of an ellipsoidal reflector which focuses the shock wave to an external focal point (F2). The ellipsoidal reflector of the research lithotripter had the same dimensions as that of the Dornier HM3 lithotripter: major half-axis a=139 mm and minor half-axis b=78 mm. The travel distance of the shock wave from the spark to the reflector, and on to F2 was $2a$= 278 mm. Assuming the speed of sound in water to be 1500 m/s, the corresponding time delay for this travel distance (i.e. spark source to target) is 185 μs.

The temporal profile of the shock pulse produced by our lithotripter has been characterized using a calibrated PVDF membrane hydrophone, and consists of a positive spike with shock front followed by a negative tail, all with a total duration of ~4 μs.[53] The experiments described in the present study were performed at a charging potential of 20 kV. At this potential the lithotripter pulse had a peak positive pressure amplitude of ~40 MPa, and a peak negative pressure amplitude of ~8 MPa. The -6 dB zone of the acoustic field of this lithotripter measured ~10 mm wide by ~60 mm axial length.

The lithotripter water tank had an optically clear glass window on a cylindrical port that extended inward, making it possible to position the lens of the HS-camera within 100 mm of F2. This did not alter the acoustic field. For all experiments the tank was filled with degassed water softened by addition of $NaHCO_3$ (conductivity ~660 μS/cm). Filtered (100 μm filter) deionized water was degassed under vacuum in a closed system for 1–2 hrs prior to filling the lithotripter tank. For these experiments water was held in the lithotripter for 4–6 hrs without further degassing. Oxygen content of the water increased during this time from ~3–4 ppm at time of filling the lithotripter, to no greater than 5.5 ppm at completion of experiments. Thus, dissolved gas and cavitation nuclei were never completely removed from the lithotripter water.

Artificial and natural stones

Two types of artificial stones prepared from gypsum cement were used. Ultracal 30™ (U-30) gypsum (United States Gypsum Company, Chicago, IL)[54] or Portland cement were mixed with deionized water (U-30 1:1; Portland 1:3); the mixture was pipeted into flat-bottom 96-well polystyrene cell culture plates (#3596 Costar, Cambridge, MA) and allowed to solidify under water overnight. The plastic was dissolved with chloroform to release the pellets. The stones were washed thoroughly with water and stored under water. U-30 stones measured approximately 6.5 mm in diameter by 7.5 mm in length. The density, longitudinal and transverse wave velocities for U-30 stones were $\rho=(1.7\pm0.1)\times10^3 kg/(m^3)$, $c_1=(3.1\pm0.3)\times10^3 m/s$, and $c_t=(1.5\pm0.3)\times10^3 m/s$, respectively, which is in the range for natural stones.[55] We have used U-30 cylinders previously as model stones in studies to assess the damage mechanisms of lithotripter shock waves.[17,56–58] The stones made from Portland cement measured approximately 6.5 mm in diameter by 10 mm in length.

Natural calcium oxalate monohydrate kidney stones were obtained from a urinary stone analytical service (Beck Analytical Services, Indianapolis, IN). Prior to use, these stones were hydrated by submersion in water for 10 days. For lithotripsy, stones were either placed atop a sheet of 4 mil thickness low-density polyethylene, or were held by a household rubber band. All image sequences show bubble activity generated by a single shock wave. Through the course of these experiments numerous recordings were made using a given stone and, typically, the single shock waves were fired minutes apart. In some cases (where specifically noted) the images capture the cavitation associated with the last shock wave of a series of shock waves fired at a pre-determined rate.

RESULTS

Bubble clusters at the stone surface were derived from individual bubbles

Analysis of sequential frames showed that the development of bubble clusters was preceded by the formation of individual bubbles. Figure 1 presents a series of frames in which the first image shows the stone at 180 μs, just at the time of the arrival of the shock wave, and before bubbles are visible. At 250 μs (frame 1b) the stone is covered by numerous small bubbles. As seen in subsequent frames, these bubbles grow and appear to aggregate to form a cluster of bubbles that overlies most of the surface of the stone, and in which many of the individual bubbles seen earlier are no longer identifiable. The coalescence of bubbles, the recruitment of

individual bubbles into a cluster, is suggested as well by images (Fig 1, frames e, f; Figs 7, 8) in which movement of the bubble cluster across the surface of the stone leaves portions of the stone bubble-free. That is, the images give the impression that individual bubbles have become caught up in the cluster and have moved from their original position.

Bubble clusters occurred reproducibly across several regions of the stone

For the majority of experiments cylindrical stones were used. The stones were positioned so that their long axis was along the acoustic axis of the lithotripter. With this orientation the stone presented a flat proximal end or face, curved sides and a flat distal end. The incoming shock wave thus hit the flat proximal end first (Fig 2a). With each lithotripter pulse there was, consistently, the formation of a population of individual bubbles that then gave rise to three main bubble clusters: one at the proximal face, one at the distal end, and one located along the sides of the stone. The bubble cluster at the proximal face (proximal cluster) (Figs 2, 3) typically formed an envelope or blister that, as it expanded, extended from the surface of the stone as much as 3 mm. It would then constrict close to its point of contact with the stone (Figs 2f, 3) and take a “mushroom cloud” shape. The cluster would collapse to a narrow (~2 mm diameter) point of impact near the center of the stone and then rebound (Fig. 4). It was this region of the proximal face that upon treatment with multiple shock waves showed damage in the form of a crater or pit (Fig 5a). The remainder of the proximal face was relatively undamaged. Thus, the formation and subsequent collapse of the bubble cluster at the proximal face of the stone appears to have involved the coalescence of numerous individual cavitation bubbles to form a large single bubble or cluster of bubbles that collapsed with damaging force.

Concurrent with the formation of the proximal bubble cluster, another cluster developed at the distal end of the stone (Figs 1, 6), and still another formed along the sides of the stone (Figs 7, 8). The distal cluster was the smallest of the three in overall area and remained centered atop the distal end of the stone. This cluster sometimes appeared to be a solitary bubble (Figs 1f, 6e, 6f) that collapsed sooner than the proximal cluster (duration of distal cluster ~400 μs, proximal cluster ~600 μs) and caused very little damage to the distal end of the stone (Fig 5b).

The cluster associated with the sides of the stone exhibited substantial movement as it retracted from the distal end, over the edge and down the sides of the stone (Figs 1f, 6c–f, 7d–e, 8d–e). Following retraction to the side of the stone this cluster formed a band or ring that appeared to extend completely around the stone (Fig 1f, 7e, 8e) and collapsed to a narrow line. Although some high-speed camera images (Figs 1g, 8g) gave the impression that sand may have been dislodged from the stone, collapse of this side-cluster did not result in erosion or pitting. Clusters at the side of the stone also appeared to coalesce with and to contribute to the cluster at the proximal end of the stone. Figures 2, 9 and 11 show cases where bubbles below the level of the rubber band swept down to join with the proximal cluster.

The occurrence of a bubble cluster at the side of the stone was a consistent feature observed for each shock wave and did not appear to be influenced by the way in which the stone was held in the lithotripter. That is, in most experiments the stones were held in position by a rubber band. However, clusters did not consistently develop in contact with the rubber band and, indeed, formed on stones that were supported by a sheet of low-density polyethylene instead of being secured by a rubber band (Fig 8).

Cavitation bubble clusters along the sides of stones interacted with fractures

Cracks perpendicular to the shock wave axis commonly developed in the target stones during shock wave treatment (Figs 9, 10, 11, 12). The fracture line was usually 2–3 mm from the distal end and, thus, in a position characteristic of failure by a spall mechanism.[7, 59–61] Cracks appeared to attract bubble cluster activity. It may not always have been possible to see existing

fractures in the recorded images, but when a fracture was observable it typically marked the site of collapse of the side-cluster. That is, when a crack was present in the stone the side-cluster developed along the crack and collapsed into it (Figs 9, 10). For example, figure 9 shows a stone that has a fracture visible about 3 mm off the distal end. In this set of images the bubble cluster at the side of the stone formed right on top of the crack (Figs 9c, d). Upon collapse the cluster disappeared into the crack (Fig 9e). The same cavitation behavior was seen with other stones in which cracks developed at different locations along the side (Figs. 10, 11, 12). Thus, superposition of the cluster over the crack did not appear to be a coincidence. That is, it did not matter whether the crack was close to the rubber band (Fig. 10, 12) or close to the distal end of the stone (Fig 9, 11), the cluster still collapsed at the crack.[34] When bubble clusters collapsed into cracks it often appeared that the cracks became wider (Figs 9, 10, 11). However, it is not clear from analysis of the images whether this bubble activity was directly responsible for widening the gap.

Bubble clusters developed at the surface of natural kidney stones

The formation of cavitation bubble clusters was not limited in occurrence to the use of artificial stones as a target. Figure 12 shows a calcium oxalate monohydrate stone in which a cluster developed over the side of the stone and subsequently collapsed along the line of a fracture. Also, in these images there is a very close correlation between the site of collapse of the side-cluster and the location of cracks that developed in the stone.

DISCUSSION

Theoretical models of cavitation and shock wave-bubble interactions generally assume bubbles to be single, spherical and relatively small,[13,38,39,41,42] but experimental studies have shown convincingly that such ideal characteristics do not always hold true.[15,32,34,36,42] Our observations with high-speed imaging reiterate these findings and go on to show in improved detail the dynamic nature of cavitation bubble activity at the surface of stones. A key observation from the present study is that the cavitation bubbles that form under influence of the tensile phase of the shock wave come to lose their identity as solitary bubbles and merge to form bubble clusters. In other words, the cavitation bubbles that form at the surface of stones do not cycle independently of one another, but instead interact as dynamic bubble clusters.

The cavitation we observed to be associated with both artificial and natural stones was characterized by the formation of bubbles that grew to cover large areas of the stone's surface. These large bubbles tended to be irregular in shape. It was not generally possible to determine whether there was a single cavity of complicated shape, or if the cavitation consisted of numerous smaller bubbles. Because the behavior of these bubbles was quite different from what has been appreciated to characterize individual, spherical cavitation bubbles, we have chosen to refer to them as "bubble clusters". Some of the original studies of multiple cavitation bubbles[46,47,62,63] used the term "cavity cluster" for what is now often referred to as "cloud cavitation".[64] The latter is typically associated with a large number of cavitation bubbles that are sufficiently dilute such that they do not directly interact with each other (coalesce), even though they may produce large dynamic effects by effectively changing the average properties and dynamics of the fluid as a whole (i.e. bubbles and liquid). The present use of the term "cluster" is thus purely descriptive and is not necessarily meant to imply any close association with the phenomena of cloud cavitation or its analytical modeling.

Bubble clusters developed consistently in several locations at the stone surface: at the proximal face, along the sides, and at the distal end of the stone. It is likely that the size and shape of a stone will influence bubble cluster behavior, and one might expect bubble dynamics to change as the stone is progressively broken into smaller fragments. In our studies with intact stones the largest bubble cluster formed at the proximal face. Since cavitation bubble expansion is

mainly dependent on the amplitude of the tensile phase of the lithotripter shock wave, bubbles would be expected to grow largest in the region of highest negative pressure. Such a region is the area immediately in front of the stone. When the pressure pulse impacts the stone, a portion of its energy is reflected. Because the water/stone interface is an acoustically hard boundary, the shock wave will reflect in phase and the negative pressure will be increased by ~60%. Cavitation may also be more prominent at the proximal face of a stone because cavitation nuclei might be more abundant in this region. That is, as the proximal face becomes etched and pitted these outward-facing defects would tend to capture cavitation nuclei.[65,66] The presence of nuclei generated by one pulse could then promote bubble growth during subsequent shock waves.[42,67]

The bubble clusters that formed in different locations appear to have contributed to stone breakage in different ways. The proximal cluster typically caused erosion or pitting at the leading face of the stone. For most stones this damage was prominent. In addition to this direct effect, cluster collapse at the proximal end of the stone likely generated a secondary shock wave of substantial magnitude. Such a shock wave originating from cluster collapse could produce pressure gradients within the stone that could contribute to breakage by other mechanisms such as spall.[7,15,54] In related experiments we have observed that although spall fracture of U-30 stones can occur at high overpressure sufficient to inhibit cavitation, distal transverse fracture of stones occurs more readily under conditions that permit cavitation at the proximal face of the stone.[17] These high-speed camera images, which show cluster collapse to be dramatic and tightly focused at the proximal end of stones, lend support to the idea of such a relationship between cavitation and spall.

Damage to the distal end of the stones was minor compared to the erosion produced at the proximal end. The bubble clusters that formed at the distal face rarely grew to more than a millimeter in height and occupied a footprint no more than several millimeters in diameter. This compares with proximal clusters that grew to cover, or even overlap, the entire 6.5 mm diameter proximal end of the stone. The shape of the clusters at collapse was also different at the two ends of the stone. Whereas the proximal cluster typically formed a mushroom shape (Fig. 2), the distal cluster sometimes gave the appearance of a single bubble that collapsed asymmetrically. For example, the sequence of frames in Figure 6 shows images that capture the coalescence of small bubbles to form a distal cluster that, just before collapse, appears to contain a vortex. This vortex form has previously been described as a characteristic of the asymmetric bubble collapse that results in focal pitting of metal targets.[1] In the present study, however, the effect of such bubbles at the distal face of the stone was unremarkable.

The collapse of bubble clusters at the sides of stones may have contributed to the growth of fractures. In many cases the direct damage caused by clusters that encircled the stone was not impressive, and appeared to consist of the loss of small amounts of sand visible as a faint mist of particles raised off the surface (e.g. Figs. 7g, 8g). In some instances, however, cluster collapse was associated with the growth of cracks. In almost all cases when a crack was already visible in the stone, the cluster developed and collapsed at that location (e.g. Figs. 9, 11). An existing crack might act as a focus for bubble cluster formation by providing a source of cavitation nuclei. A crack might physically stabilize cavitation bubbles,[65,66,68] keeping them from being swept away by fluid motion induced by bubble dynamics elsewhere on the stone. It has also been suggested that cavitation associated with a crack or crevice could produce large tensile stresses during rebound and thereby contribute to crack growth.[51]

These HS-camera observations do not rule out the possibility that cavitation may have been involved in the initiation of new fractures. Sass *et al.*[34] have suggested this as a potential mechanism for shock wave damage to gallstones. The series of images in Figure 12 (left column) shows a close correlation between the position of cluster collapse and the formation

of a crack in a natural stone that does not become obvious until the next shock wave (Fig. 12, right column). Image resolution is a limitation here. It may be that a microscopic fracture existed prior to the first shock wave of the two and did not grow to visible size until the subsequent shot. What seems most reasonable to conclude is that, overall, the images demonstrate that bubble clusters are associated with fractures in stones and that cluster collapse along the line of a fracture may promote its growth.

Previous studies using high-speed imaging have demonstrated the formation and collapse of cavitation bubbles at the surface of natural and artificial stones. Sass *et al.*[34] used a high-speed camera system capable of capturing sequential images at 100 μs steps — comparable to the frame rate we used for the present study. Some of their observations seem to correlate well with our findings. For example, they demonstrate greater bubble activity at the proximal face than elsewhere on the stone, and they suggest that bubbles appeared to fuse at this leading face of the stone. However, the images give no indication of the recruitment of individual bubbles to form aggregates or clusters, and do not show evidence of the dynamic movement of bubbles across the surface of the stone that characterized bubble behavior in our experiments. In a recent study Xi and Zhong[36] used fast frame photoelastic imaging to capture cavitation bubble activity at the surface of epoxy model stones. They recorded single frames with each lithotripter pulse and staggered the shutter delay time in order to build a sequence over the lifetime of the bubble cycle. These images with high contrast and good resolution show two-dimensional profiles of bubble growth at the surface of the blocks. In some sequences bubbles enlarge and grow to fully surround the target. Later frames show bubbles primarily at the proximal and distal sides. The images capture profiles in just two dimensions, so it is difficult to appreciate bubble movement; however, these profiles support the idea that bubbles coalesce to cover large areas of the target.

In summary, these observations with high speed imaging lead to several conclusions about the characteristics of the cavitation associated with stones, and the role that cavitation bubbles play in stone fragmentation in SWL. The data show that cavitation bubble activity at the surface of stones in vitro is dominated by the formation of bubble clusters. Cluster formation involves the aggregation of many individual cavitation bubbles. Clusters grow and shift dramatically in position, sweep across the surface of the stone and collapse at discrete foci. Separate clusters develop over different regions of the stone, and contribute to stone breakage in different ways. The cluster that develops and collapses at the proximal end of the stone is the largest and causes prominent pitting at that leading face. Bubble clusters consistently form, also, at the distal end of the stone and along the sides of the stone. Cluster formation occurs with natural stones as well as with artificial stones. Cracks that develop in a stone attract bubble cluster activity, and cavitation along an existing fracture may help such fractures to grow. Thus, our observations lend further support to the well-established idea that cavitation contributes to stone comminution through erosion and pitting, and also suggest that cavitation bubble cluster activity may be involved in the growth of fractures in stones treated by shock wave lithotripsy.

Acknowledgements

This research was supported by NIH grants DK43881 and DK55674 and by a grant from the Whitaker Foundation.

References

1. Crum LA. Cavitation microjets as a contributory mechanism for renal calculi disintegration in ESWL. J Urol 1988;140:1587–1590. [PubMed: 3057239]
2. Delius M. Minimal static excess pressure minimises the effect of extracorporeal shock waves on cells and reduces it on gallstones. Ultrasound Med Biol 1997;23:611–617. [PubMed: 9232770]
3. Sass W, Dreyer HP, Kettermann S, Seifert J. The role of cavitational activity in fragmentation processes by lithotripters. J Stone Dis 1992;4:193–207. [PubMed: 10147666]

4. Vakil N, Everbach EC. Transient acoustic cavitation in gallstone fragmentation: a study of gallstones fragmented in vivo. Ultrasound Med Biol 1993;19:331–342. [PubMed: 8346607]
5. Zhong P, Cioanta I, Cocks FH, Preminger GM. Inertial cavitation and associated acoustic emission produced during electrohydraulic shock wave lithotripsy. J Acoust Soc Am 1997;101:2940–2950. [PubMed: 9165740]
6. Zhong P, Cocks FH, Cioanta I, Preminger GM. Controlled, forced collapse of cavitation bubbles for improved stone fragmentation during shock wave lithotripsy. 1997;158:2323–2328.
7. Zhu S, Cocks FH, Preminger GM, Zhong P. The role of stress waves and cavitation in stone comminution in shock wave lithotripsy. Ultrasound Med Biol 2002;28:661–671. [PubMed: 12079703]
8. Carstensen EL, Gracewski S, Dalecki D. The search for cavitation in vivo. Ultrasound Med Biol 2000;26:1377–1385. [PubMed: 11179611]
9. Coleman AJ, Choi MJ, Saunders JE. Detection of acoustic emission from cavitation in tissue during clinical extracorporeal lithotripsy. Ultrasound Med Biol 1996;22:1079–1087. [PubMed: 9004432]
10. Delius M, Ueberle F, Eisenmenger W. Extracorporeal shock waves act by shock wave-gas bubble interaction. Ultrasound Med Biol 1998;24:1055–1059. [PubMed: 9809639]
11. Evan AP, Willis LR, McAteer JA, Bailey MR, Connors BA, Shao Y, Lingeman JE, Williams JC Jr, Fineberg NS, Crum LA. Kidney damage and renal functional changes are minimized by waveform control that suppresses cavitation in SWL. J Urol 2002;168:1556–1562. [PubMed: 12352457]
12. Sapozhnikov OA, Bailey MR, Crum LA, Miller NA, Cleveland RO, Pishchalnikov YA, Pishchalnikova IV, McAteer JA, Connors BA, Blomgren PM, Evan AP. Ultrasound guided localized detection of cavitation during lithotripsy in pig kidney in vivo. Proc IEEE Ultrasonics Symp 2001:1437–1440.
13. Zhong P, Zhou Y, Zhu S. Dynamics of bubble oscillation in constrained media and mechanisms of vessel rupture in SWL. Ultrasound Med Biol 2001;27:119–134. [PubMed: 11295278]
14. Vakil N, Gracewski SM, Everbach EC. Relationship of model stone properties to fragmentation mechanisms during lithotripsy. J litho Stone Dis 1991;3:304–310.
15. Zhong P, Chuong CJ, Preminger GM. Propagation of shock waves in elastic solids caused by cavitation microjet impact. II: Application in extracorporeal shock wave lithotripsy. J Acout Soc Am 1993;94:29–36.
16. Holmer NG, Almquist LO, Hertz TG, Holm A, Lindstedt E, Persson HW, Hertz CH. On the mechanism of kidney stone disintegration by acoustic shock waves. Ultrasound Med Biol 1991;17:479–489. [PubMed: 1962349]
17. McAteer JA, Cleveland RO, Rietjens DL, Pishchalnikov YA, Pishchalnikova IV, Williams JC Jr. Cavitation promotes spall failure of model kidney stones treated by shock wave lithotripsy *in vitro*. Proc 17th Int'l Congress Acoust 2002;VII:188–189.
18. Bailey MR. Acoustic and cavitation fields of a pressure release ellipsoidal reflector. J Acoust Soc Am 1997;101:3138.abstr
19. Cathignol D, Tavakkoli J, Birer A, Arefiev A. Comparison between the effects of cavitation induced by two different pressure-time shock waveform pulses. IEEE Trans Ultrason Ferroelectr Freq Control 1998;45:788–799. [PubMed: 18244230]
20. Bailey, MR. Ph.D. Thesis, Technical Report ARL-TR-97-1, Applied Research Laboratories. The University of Texas at Austin; 1997. Control of acoustic cavitation with application in lithotripsy.
21. Sokolov DL, Bailey MR, Crum LA. Use of a dual-pulse lithotripter to generate a localized and intensified cavitation field. J Acoust Soc Am 2001;110:1685–1695. [PubMed: 11572377]
22. Zhong P, Zhou Y. Suppression of large intraluminal bubble expansion in shock wave lithotripsy without compromising stone comminution: Methodology and *in vitro* experiments. J Acoust Soc Am 2001;110:3283–3291. [PubMed: 11785829]
23. Bailey MR, Blackstock DT, Cleveland RO, Crum LA. Comparison of electrohydraulic lithotripters with rigid and pressure-release ellipsoidal reflectors: II. Cavitation fields J Acoust Soc Am 1999;106:1149–1160.
24. Coleman AJ, Saunders JE, Crum LA, Dyson M. Acoustic cavitation generated by an extracorporeal shockwave lithotripter. Ultrasound Med Biol 1987;13:69–76. [PubMed: 3590362]
25. Lifshitz DA, Williams JC Jr, Sturtevant B, Conners BA, Evan AP, McAteer JA. Quantization of shock wave cavitation damage *in vitro*. Ultrasound Med Biol 1997;23:461–471. [PubMed: 9160914]

26. Delacretaz G, Rink K, Pittomvils G, Lafaut JP, Vandeursen H, Boving R. Importance of the implosion of ESWL-induced cavitation bubbles. Ultrasound Med Biol 1995;21:97–103. [PubMed: 7754583]
27. Huber P, Debus J, Peschke P, Hahn EW, Lorenz WJ. In vivo detection of ultrasonically induced cavitation by a fibre-optic technique. Ultrasound Med Biol 1994;20:811–825. [PubMed: 7863570]
28. Coleman AJ, Choi MJ, Saunders JE, Leighton TG. Acoustic emission and sonoluminescence due to cavitation at the beam focus of an electrohydraulic shock wave lithotripter. Ultrasound Med Biol 1992;18:267–281. [PubMed: 1595133]
29. Coleman AJ, Whitlock M, Leighton T, Saunders JE. The spatial distribution of cavitation induced acoustic emission, sonoluminescence and cell lysis in the field of a shock wave lithotripter. Phys Med Biol 1993;38:1545–1560. [PubMed: 8272431]
30. Matula TJ, Hilmo PR, Bailey MR, Crum LA. In vitro sonoluminescence and sonochemistry studies with an electrohydraulic shock wave lithotripter. Ultrasound Med Biol 2002;28:1199–1207. [PubMed: 12401391]
31. Jöchle K, Debus J, Lorenz WJ, Huber P. A new method of quantitative cavitation assessment in the field of a lithotripter. Ultrasound Med Biol 1996;22:329–338. [PubMed: 8783465]
32. Huber P, Debus J, Jöchle K, Simiantonakis I, Jenne J, Rastert R, Spoo J, Lorenz WJ, Wannenmacher M. Control of cavitation activity by different shockwave pulsing regimes. Physics Med Biol 1999;44:1427–1437.
33. Cleveland RO, Sapozhnikov OA, Bailey MR, Crum LA. A dual passive cavitation detector for localized detection of lithotripsy-induced cavitation *in vitro*. J Acoust Soc Am 2000;107:1745–1758. [PubMed: 10738826]
34. Sass W, Braunlich M, Dreyer HP, Matura E, Folberth W, Priesmeyer HG, Seifert J. The mechanisms of stone disintegration by shock waves. Ultrasound Med Biol 1991;17:239–243. [PubMed: 1887509]
35. Carnell MT, Emmony DC. A schlieren study of the interaction between a lithotripter shock wave and a simulated kidney stone. Ultrasound Med Biol 1995;21:721–724. [PubMed: 8525563]
36. Xi X, Zhong P. Dynamic photoelastic study of the transient stress field in solids during shock wave lithotripsy. J Acoust Soc Am 2001;109:1226–1239. [PubMed: 11303936]
37. Vogel A, Busch S, Parlitz U. Shock wave emission and cavitation bubble generation by picosecond and nanosecond optical breakdown in water. J Acoust Soc Am 1996;100:148–165.
38. Choi MJ, Coleman AJ, Saunders JE. The influence of fluid properties and pulse amplitude on bubble dynamics in the field of a shock wave lithotripter. Phys Med Biol 1993;38:1561–1573. [PubMed: 8272432]
39. Church CC. A theoretical study of cavitation generated by an extracorporeal shock wave lithotripter. J Acoust Soc Am 1989;86:215–227. [PubMed: 2754108]
40. Ding Z, Gracewski SM. Response of constrained and unconstrained bubbles to lithotripter shock wave pulses. J Acoust Soc Am 1994;96:3636–3644. [PubMed: 7814766]
41. Matula TJ, Hilmo PR, Storey BD, Szeri AJ. Radial response of individual bubbles subjected to shock wave lithotripsy pulses *in vitro*. Physics Fluids 2002;14:913–921.
42. Sapozhnikov OA, Khokhlova VA, Bailey MR, Williams JC Jr, McAteer JA, Cleveland RO, Crum LA. Effect of overpressure and pulse repetition frequency on cavitation in shock wave lithotripsy. J Acoust Soc Am 2002;112:1183–1195. [PubMed: 12243163]
43. Zhu S, Zhong P. Shock wave-inertial microbubble interaction: a theoretical study based on the Gilmore formulation for bubble dynamics. J Acoust Soc Am 1999;106:3024–3033. [PubMed: 10573912]
44. Kodama T, Takayama K. Dynamic behavior of bubbles during extracorporeal shock-wave lithotripsy. Ultrasound Med Biol 1998;24:723–738. [PubMed: 9695276]
45. Lauterborn W, Ohl CD. Cavitation bubble dynamics. Ultrasonics Sonochem 1997;4:65–75.
46. Morch, KA. On the collapse of cavity clusters in flow cavitation. In: Lauterborn, W., editor. Cavitation and Inhomogeneities in Underwater Acoustics. Springer-Verlag; 1980. p. 95-100.
47. Morch KA. Cavity cluster dynamics and cavitation erosion. Proc ASME Cavitation and Polyphase Flow Forum 1981:1–10.
48. Omta R. Oscillations of a cloud of bubbles of small and not so small amplitude. J Acoust Soc Am 1987;82:1018–1033.

49. Reisman GE, Wang YC, Brennen CE. Observations of shock waves in cloud cavitation. J Fluid Mech 1998;355:255–283.
50. Smereka P, Banerjee S. The dynamics of periodically driven bubble clouds. Phys Fluids 1988;31:3519–3541.
51. Field JE. The physics of liquid impact, shock wave interactions with cavities, and the implications to shock wave lithotripsy. Phys Med Biol 1991;36:1475–1484. [PubMed: 1754618]
52. Tanguay M, Colonius T. Numerical investigation of bubble cloud dynamics in shock wave lithotripsy. Proc ASME Fluids Eng Div 2002:FEDSM2002–31010.
53. Cleveland RO, Bailey MR, Hartenbaum B, Lokhandwalla M, McAteer JA, Sturtevant B. Design and characterization of a research electrohydraulic lithotripter patterned after the Dornier HM3. Rev Scientific Instr 2000;71:2514–2525.
54. Gracewski SM, Dahake G, Ding Z, Burns SJ, Everbach EC. Internal stress wave measurements in solids subjected to lithotripter pulses. J Acoust Soc Am 1993;94:652–661. [PubMed: 8370871]
55. Heimbach D, Munver R, Zhong P, Jacobs J, Hesse A, Muller SC, Preminger GM. Acoustic and mechanical properties of artificial stones in comparison to natural kidney stones. J Urol 2000;164:527–544.
56. McAteer JA, Cleveland RO, Paterson RF, Rietjens DL, Evan AP, Connors BA, Lingeman JE, Pishchalnikov YA, Pishchalnikova IV, Williams JC Jr. Evidence that cavitation and spall contribute to stone failure in an animal model of kidney stone fragmentation by shock wave lithotripsy (SWL). Proc 17th Int'l Congress Acoust 2002;VII:202–203.
57. McAteer JA, Paterson RF, Lifshitz DA, Lingeman JE, Rietjens DL, Connors BA, Evan AP, Williams JC Jr. *In vitro* model of shock wave lithotripsy (SWL) produces stone breakage equivalent to that seen in vivo. Proc 17th Int'l Congress Acoust 2002;VII:180–182.
58. Paterson RF, Lifshitz DA, Lingeman JE, Williams JC Jr, Rietjens DL, Evan AP, Connors BA, Bailey MR, Crum LA, Cleveland RO, Pishchalnikov YA, Pishchalnikova IV, McAteer JA. Slowing the pulse repetition frequency in shock wave lithotripsy (SWL) improves stone fragmentation in vivo. Proc 17th Int'l Congress Acoust 2002;VII:200–201.
59. Cleveland RO, McAteer JA, Muller R. Time-lapse nondestructive assessment of shock wave damage to kidney stones *in vitro* using micro-computed tomography. J Acoust Soc Am 2001;110:1733–736. [PubMed: 11681352]
60. Cleveland RO, McAteer JA, Williams JC Jr. Correlation between the predicted stress field and observed spall-failure in artificial kidney stones treated by shock wave lithotripsy (SWL) in vitro. Proc 17th Int'l Congress Acoust 2002;VII:174–175.
61. Zhong P, Preminger GM. Mechanisms of differing stone fragility in extracorporeal shockwave lithotripsy. J Endourol 1994;8:263–268. [PubMed: 7981735]
62. Dear JP, Field JE. A study of the collapse of the arrays of cavities. J Fluid Mech 1988;190:409–425.
63. Hansson I, Morch KA. The dynamics of cavity clusters in ultrasonic (vibratory) cavitation erosion. J Appl Phys 1980;51:4651–4658.
64. Brennen, CE. Cavitation and Bubble Dynamics. Oxford University Press; 1985.
65. Bailey MR, Cleveland RO, Sapozhnikov OA, McAteer JA, Williams JC Jr, Crum LA. Effect of increased ambient pressure on lithotripsy-induced cavitation in bulk fluid and at solid surfaces. J Acoust Soc Am 1999;105:1267–1270.
66. Cleveland RO, Bailey MR, Crum LA, Stonehill MA, Williams JC Jr, McAteer JA. Effect of overpressure on dissolution and cavitation of bubbles stabilized on a metal surface. Proc 135th Acoust Soc Am 1998;4:2499–2500.
67. Delius M, Brendel W. A model of extracorporeal shock wave action: tandem action of shock waves. Ultrasound Med Biol 1988;14:515–518. [PubMed: 3227574]
68. Crum LA. Tensile strength of water. Nature 1979;278:148–149.

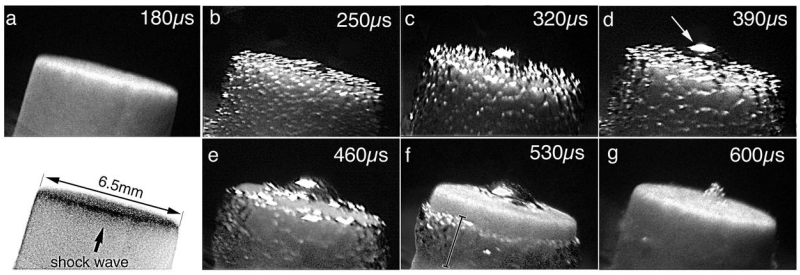

Figure 1. Individual cavitation bubbles contributing to the formation of bubble clusters at the surface of an artificial stone

This series of frames captured at 70 μs steps shows cavitation bubble activity generated by a single lithotripter pulse. The images focus on the distal one-third of the stone. The axis of shock wave propagation was nearly vertical upward (see inset). (a): This frame shows the stone at the time of shock wave arrival, but prior to the formation of cavitation bubbles. (b): 70μs after passage of the shock wave, numerous individual cavitation bubbles have formed on the surface of the stone. (c-d): The bubbles have enlarged and have begun to coalesce into a cluster. There is a prominent bubble (arrow) visible at the center of the distal surface of the stone. (e): A portion of the bubble cluster has begun to move from the end of the stone to the lateral stone surface. (f): The bubbles in this field have now divided into two separate clusters; one, possibly a single bubble at the center of the distal end of the stone, and one (bracket) forming a ring or band that appears to encircle the stone. (g): In this final frame both the distal bubble and the cluster along the sides of the stone have collapsed.

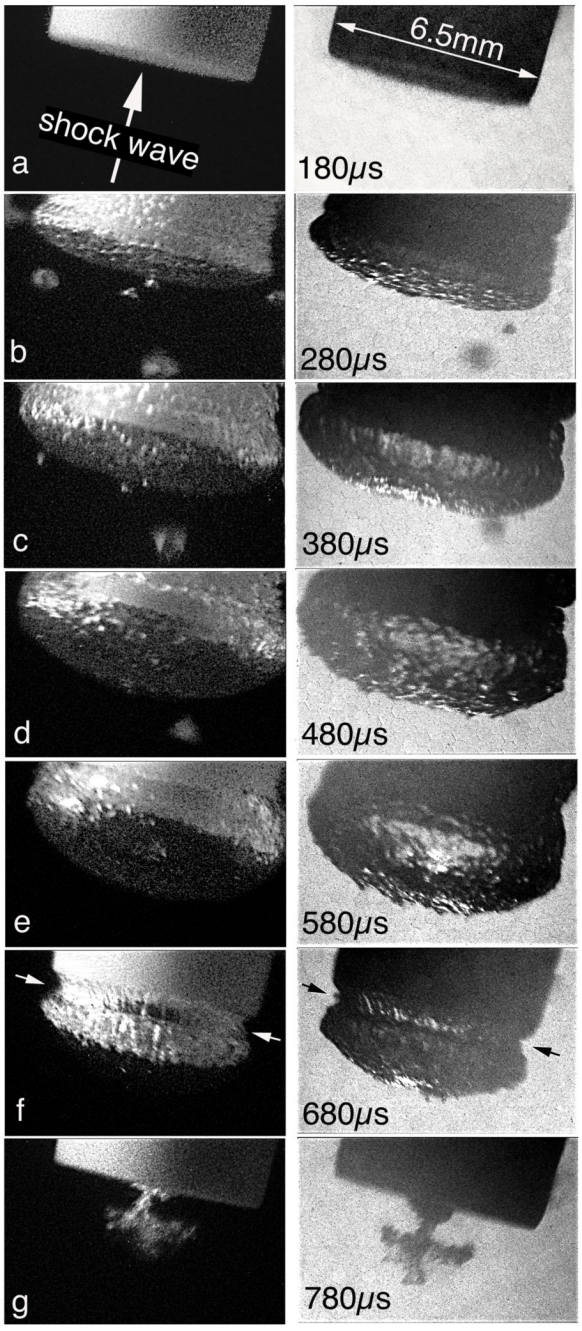

Figure 2. Bubble cluster formation and collapse at the proximal face of a stone

These images, captured at 100 μs steps, show the growth of the bubble cluster that consistently formed at the leading face of the stone. Two different stones are shown and images were recorded using different illumination. In the left column illumination was from the side and in the right column the lamp was positioned at the back. By side lighting the stone is light and the bubbles are transparent. By back lighting the stone is dark and the bubbles are opaque. (a): These frames show the stone at the time of shock wave arrival, and thus before cavitation bubbles have formed. The arrow shows the direction of pulse propagation. (b-d): This series shows formation and growth of the cluster over the leading face of the stone. With side lighting (left) one can see numerous small bubbles at the surface of the stone and caught up by the

expanding cluster. By back lighting (right) the surface of the cluster appears rough. (e): The cluster has now expanded to extend ~3 mm off the surface of the stone. With side lighting (left) one can see that the bubble both overlaps the edge of the stone and extends up the sides. It is difficult in either frame to resolve individual bubbles within the cluster. (f): The cluster has begun to collapse. It has retracted from the sides of the stone and is constricted at its base (arrowheads). (g): The cluster has collapsed at the center of the proximal face of the stone. Note: The time from impact of the shock wave to initial collapse of the proximal cluster was approximately 600 μs. This compares with a cavitation cycle for individual bubbles in the surrounding water of approximately 300 μs.[42,65]

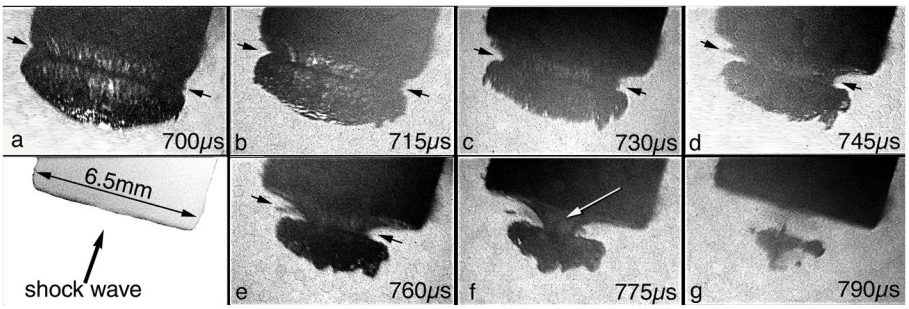

Figure 3. Details of bubble cluster collapse at the proximal face of a stone

This series of images shows 15μs steps beginning at 700 μs after spark discharge. This sequence therefore corresponds, approximately, to the interval between frames “f” and “g” of Figure 2. The collapse times of the bubble clusters in Figures 2 and 3 differ slightly. This is typical of the shot-to-shot variability in shock pulse amplitude that has been documented for electrohydraulic lithotripters.[28,33] (a-e): The bubble cluster constricts at its base (arrowheads), while the dome or cap gets smaller at a slower rate. (f): The cluster now consists of a cap and narrow stalk (arrow), with the stalk centered over the proximal face of the stone. (g): The stalk is no longer visible and just a portion of the cluster cap remains. The faint shadow visible between the stone and cluster may be debris eroded from the stone due to impact from collapse of the cluster.

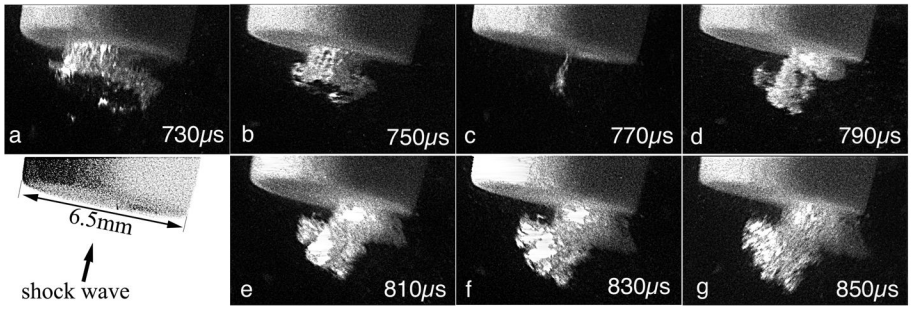

Figure 4. Cavitation bubble rebound following cluster collapse at the proximal face of the stone

This set of images demonstrates bubble rebound following initial collapse of the bubble cluster. The frames were captured in 20 μs steps, and the first frame corresponds to approximately the same point in development of the proximal bubble cluster as is shown in Figure 3c. (a-b): The cluster is collapsing a little off center. (c): Collapse is nearly complete and just a wisp of the cluster remains. (d-g): The rebounding cluster grows outward. It is difficult to identify debris that might be carried within the cluster. Note: This figure shows the last of a series of 10 shock waves delivered at a rate of 5 Hz. Bubble cluster formation, growth, collapse and rebound were observed regardless of the pulse repetition frequency.

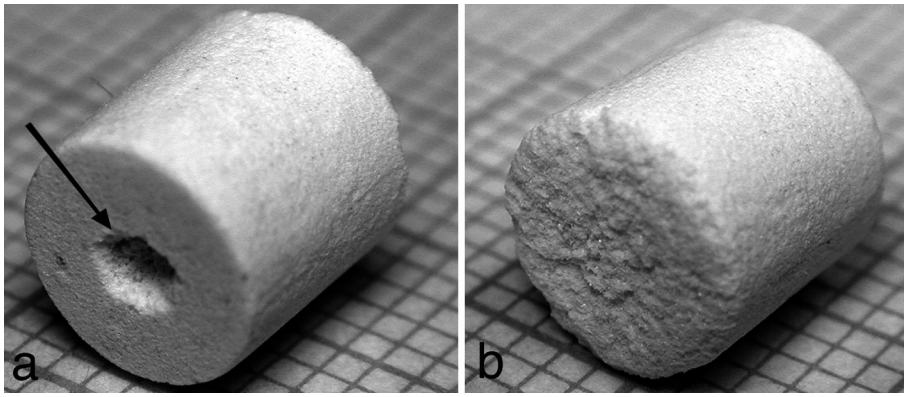

Figure 5. Cavitation damage to an artificial stone

(a): This image shows the proximal surface of a U-30 artificial stone treated with 50 shock waves delivered at 20 kV, 0.5 Hz. Cavitation bubble cluster activity has created a 2 mm diameter crater centered at the proximal end of the stone (arrow) (background grid 1 mm). (b): The distal end of the stone shows very little damage. There is no focus of erosion on the distal surface as is seen at the proximal end (frame “a”). Note: The distal ends of U-30 stones are always somewhat rougher than the proximal ends, as the distal end is not in contact with the plastic mold used to cast the stone.

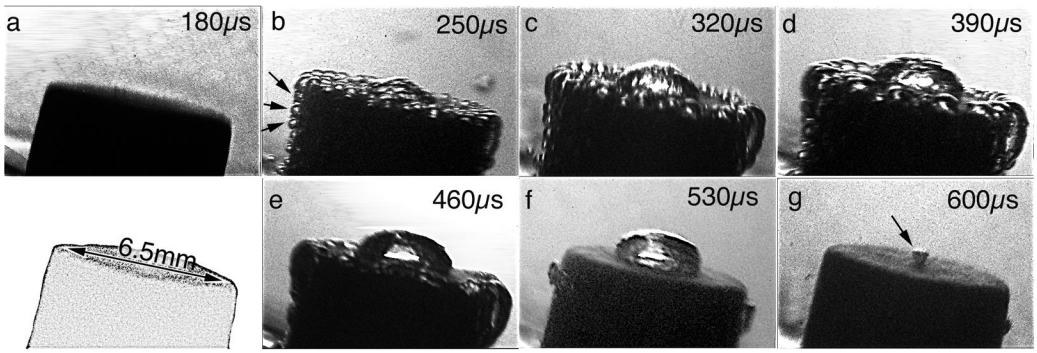

Figure 6. Cavitation bubble activity at the distal end of a stone

This set of images captures cavitation bubble activity at the distal one-third of an artificial stone. This is the same stone shown in Figure 1, but with illumination from a different angle. The timing of frames is the same as Figure 1 (i.e. 70 μs steps, beginning at 180 μs). (a): This frame, included for reference, shows the stone at the time of shock wave arrival, but before cavitation bubbles have developed. (b-d): These frames capture the formation of individual bubbles and their subsequent growth. Backlighting helps one see the boundaries of individual bubbles at the edge of the stone (arrowheads), but obscures detail elsewhere. (e-f): The "bubble cluster" shown here atop the distal end of the stone looks like it may be a solitary bubble. At its maximum expansion, this bubble extends a little more than 1 mm above the surface of the stone. This distal bubble cluster is thus much smaller than the cluster that develops at the proximal end of the stone (Fig 2, 3, 9–11). The structure of this bubble seems very similar to the shape attributed to asymmetric bubble collapse.[1] (g): This final frame has captured what remains of the distal bubble cluster (arrow) as it collapses at the center of the stone.

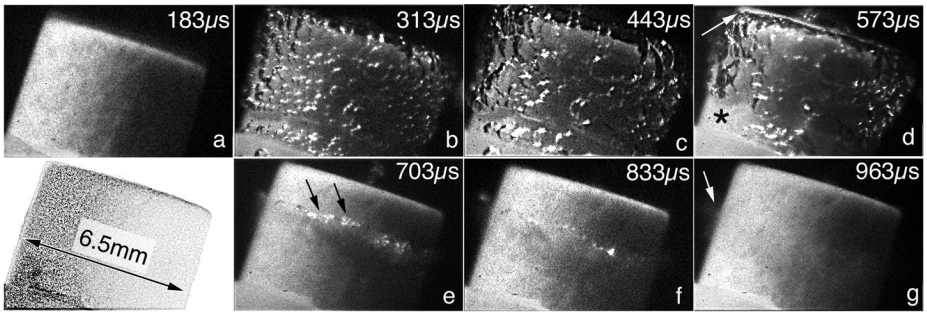

Figure 7. Bubble cluster formation and collapse at the sides of an artificial stone

This series of images shows the upper half (distal half) of a stone held in position with a rubber band (seen in lower left corner of each frame). The shock wave entered from the bottom of the stone. Frames were captured at 130 μs steps. (a): Image of the stone at the time of shock wave impact, but before bubbles are visible. (b-c): These frames show the formation and enlargement of a bubble cluster that surrounds the stone. (d): The bubble cluster has begun to retract, exposing the mid-portion (asterisk) and the distal edge (arrow) of the stone. (e-f): The cluster now forms a narrow ring or band of bubbles (arrow) 1–2 mm below the distal end. (g): In this final frame there is very faint dust near the line of cluster collapse, suggestive of fine debris released from the surface of the stone.

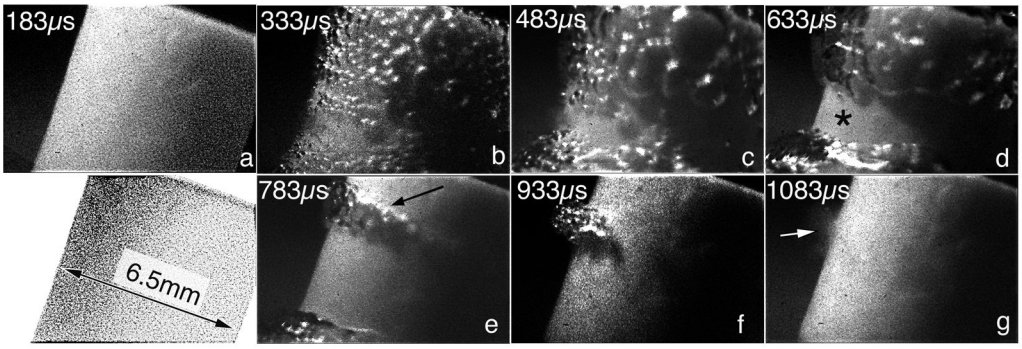

Figure 8. Bubble cluster formation on a stone not held by a ligature

This series of images shows an artificial stone that was positioned at the focus of the lithotripter by standing it upright atop a sheet of low density polyethylene. Frames were captured at 150 μs steps. These images demonstrate that formation of a bubble cluster at the side of the stone was not an artifact of the way in which the stone was held in the lithotripter (a): Stone at the time of shock wave arrival. (b-f): These frames show the formation of the bubble cluster to cover the surface of the stone, retraction of the cluster from the mid-portion (asterisk) and distal end of the stone to form a narrow band of bubbles (arrow), and collapse of those bubbles. (g): As in Figure 6, frame “g”, this image shows dust (arrow) that may be fine debris coming from the surface of the stone.

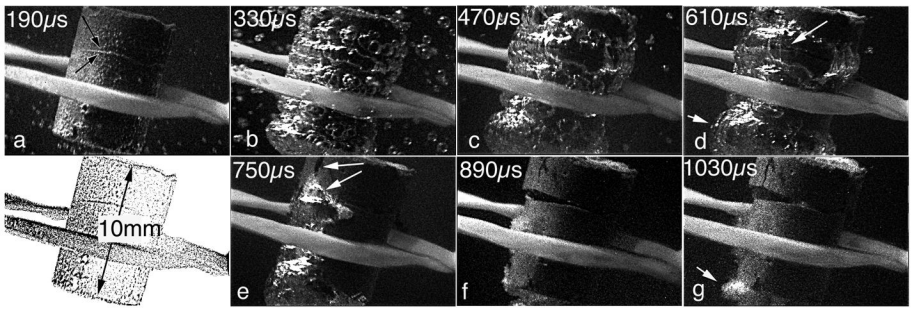

Figure 9. Bubble cluster collapse along an existing spall fracture in an artificial stone

This series of images captured at 140μs steps shows bubble cluster activity associated with a distal fracture that was present before the arrival of the shock wave. The stone is held in place by a rubber band. (a): This image shows the stone at 190 μs after spark discharge, approximately 10 μs later than the initial frames shown in figures 1, 2, 6, 7, and 8. As such, bubbles are already visible in the surrounding water, and some may be present at the surface of the stone as well. There is a transverse crack visible above the rubber band (arrows). This crack was present prior to this shot. (b-c): Bubbles grow at the surface of the stone and coalesce to form a large bubble cluster that surrounds most of the stone. (d): In this image the crack is visible (arrow) beneath the cluster at the side of the stone. The crack appears to have widened. Note also, the large proximal cluster in this frame (arrowhead). (e): The bubble cluster at the side of the stone has collapsed along the line of the transverse crack. A vertical crack is now visible as well and a portion of the cluster overlies this crack (arrow). The proximal cluster is retracting toward the leading face of the stone. (f): The crack is now considerably wider than before. (g): This frame shows bubble rebound at the proximal face of the stone (arrow).

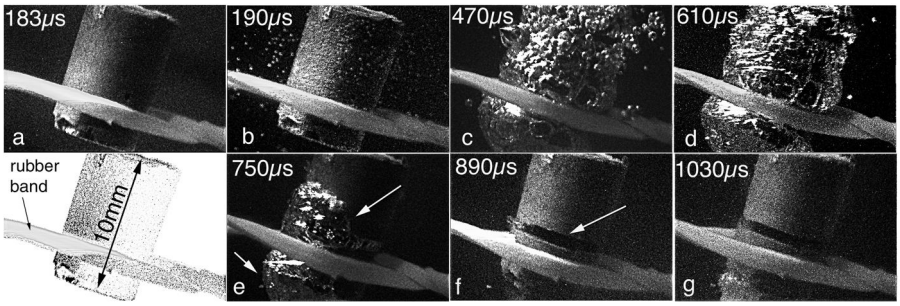

Figure 10. Superposition of bubble clusters with fracture lines is not accidental

These images are of an artificial stone in which a spall-type fracture developed low on the stone. In this case the bubble cluster still formed along the crack and appeared to collapse into it. Steps after frame "b" are 140 μs. (a): Stone prior to the arrival of the shock wave. (b): Bubbles have begun to form at the surface of the stone and in the surrounding water. (c-d): Growth of a bubble cluster that appears to completely surround the stone. (e): This frame shows a bubble cluster at the side of the stone and one at the proximal end of the stone (arrow). The side cluster has a narrow portion that runs transversely across the stone. One cannot see what lies beneath the cluster, but this is the position of a crack that is visible in frame "f". Thus, the bubble cluster appears to be collapsing into a crack. (f-g): The cluster is gone and the crack is now visible just above the rubber band (arrow).

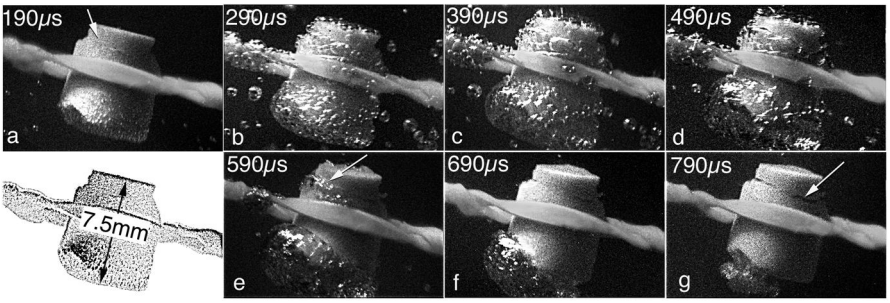

Figure 11. Bubble cluster activity over different regions of a stone

This set of images captured at 100 μs steps illustrates cavitation bubble cluster activity over different regions of a stone following a single lithotripter pulse. (a): This initial frame at 190 μs shows small bubbles at the surface of the stone, and in the surrounding water. This stone has already been damaged by previous exposure to shock waves. There is a faint fracture about 1 mm from the distal end (arrow). (b-d): Bubbles grow, and coalesce with one another to form a prominent cluster at the proximal end, a smaller cluster at the distal end and a cluster surrounding the mid-portion of the stone. (e): The bubbles above the rubber band are lined up (arrow) along the transverse fracture first visible in frame “a”. The proximal cluster is very large. (f): The proximal cluster is smaller— has begun to collapse. (g): The crack near the distal end of the stone has widened (arrow) while the proximal cluster appears much smaller — consistent with continuation of collapse or subsequent rebound.

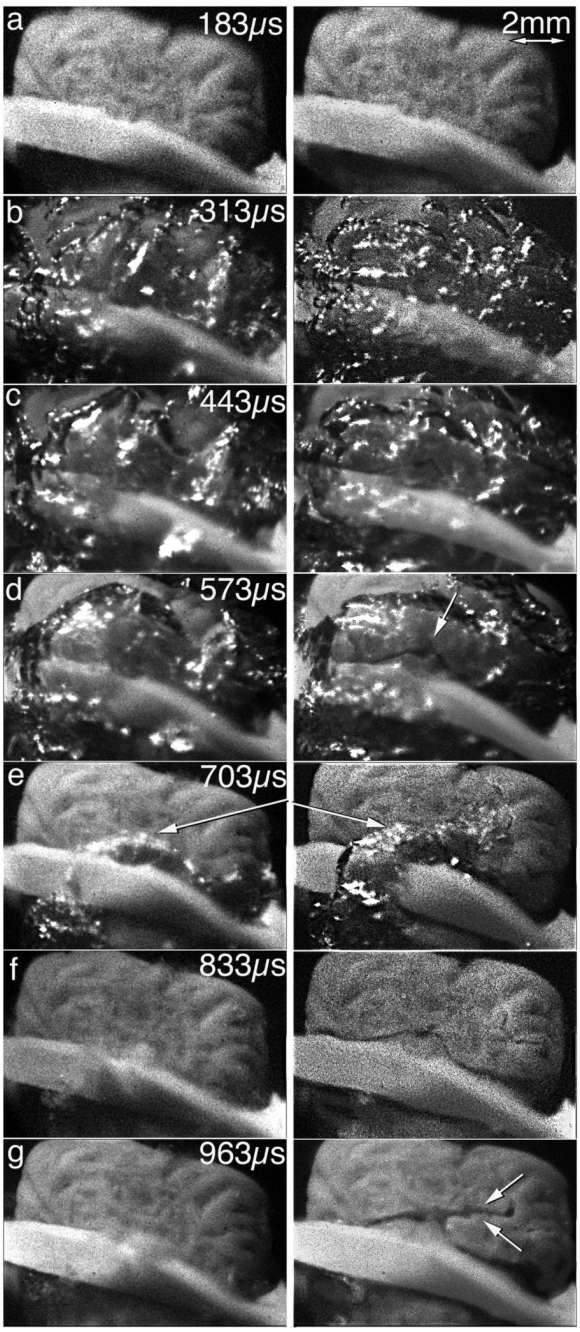

Figure 12. Cavitation bubble cluster activity at the surface of a natural kidney stone

These frames show bubble activity at the surface of a calcium oxalate monohydrate kidney stone. They demonstrate that bubble clusters form in association with natural stones, not just with artificial stones as illustrated in figures 1–11. The images are from two successive shock waves (left column = shot number 3; right column = shot number 4) fired several minutes apart, but imaged at the same framing rate (130 μs steps). Reading down, one can see the progression of bubble activity during one shot. Reading across, one can compare bubble behavior from one shock wave to the next. Note the similarity of size and location of the bubble clusters that formed with each of the two shock waves. Note also that the bubble cluster collapses along the line of a crack that becomes visible following the second shock wave and that the crack

continues to grow after cluster collapse has occurred. (a): Stone at the time of arrival of the shock wave. (b-c): A bubble cluster forms at the side of the stone, retracts from the distal end of the stone and forms a band that appears to extend around the stone. (d): The cluster in the 4^{th} shot (right column) overlies a prominent crack (arrow) that is first visible in the previous frame, frame “c”. (e): The line of bubble collapse in these two frames is very similar. For shot 4 (right column) the location of the bubble correlates well with the crack that was visible in earlier frames, and is easily seen in frames “f” and “g”. In shot 3 (left column) no crack is visible, but the cluster (arrow) is collapsing along a line that seems to correlate well with the location of the fracture that developed during shot 4. (f): Frame corresponds to the time of collapse of the proximal cluster (out of field of view). (g): Crack has widened and a segment of this crack (arrows) is now visible after the time of cluster collapse.